Extracting 2D IR frequency-frequency correlation functions from two component systems

Emily E. Fenn and M. D. Fayer[a)]
Department of Chemistry, Stanford University, Stanford, California 94305, USA

(Received 22 June 2011; accepted 25 July 2011; published online 15 August 2011)

The center line slope (CLS) method is often used to extract the frequency-frequency correlation function (FFCF) from 2D IR spectra to delineate dynamics and to identify homogeneous and inhomogeneous contributions to the absorption line shape of a system. While the CLS method is extremely efficient, quite accurate, and immune to many experimental artifacts, it has only been developed and properly applied to systems that have a single vibrational band, or to systems of two species that have spectrally resolved absorption bands. In many cases, the constituent spectra of multiple component systems overlap and cannot be distinguished from each other. This situation creates ambiguity when analyzing 2D IR spectra because dynamics for different species cannot be separated. Here a mathematical formulation is presented that extends the CLS method for a system consisting of two components (chemically distinct uncoupled oscillators). In a single component system, the CLS corresponds to the time-dependent portion of the normalized FFCF. This is not the case for a two component system, as a much more complicated expression arises. The CLS method yields a series of peak locations originating from slices taken through the 2D spectra. The slope through these peak locations yields the CLS value for the 2D spectra at a given T_w. We derive analytically that for two component systems, the peak location of the system can be decomposed into a weighted combination of the peak locations of the constituent spectra. The weighting depends upon the fractional contribution of each species at each wavelength and also on the vibrational lifetimes of both components. It is found that an unknown FFCF for one species can be determined as long as the peak locations (referred to as center line data) of one of the components are known, as well as the vibrational lifetimes, absorption spectra, and other spectral information for both components. This situation can arise when a second species is introduced into a well characterized single species system. An example is a system in which water exists in bulk form and also as water interacting with an interface. An algorithm is presented for back-calculating the unknown FFCF of the second component. The accuracy of the algorithm is tested with a variety of model cases in which all components are initially known. The algorithm successfully reproduces the FFCF for the second component within a reasonable degree of error. © *2011 American Institute of Physics*. [doi:10.1063/1.3625278]

I. INTRODUCTION

2D IR vibrational spectroscopy has proven to be an extremely powerful technique for elucidating molecular dynamics and understanding congested spectra of condensed matter systems.[1,2] Through analysis of the 2D spectral line shapes and other experimental observables, the frequency-frequency correlation function (FFCF) can be determined.[3–10] The frequency-frequency correlation function describes the likelihood that an oscillator of a certain frequency will have the same frequency after a given period of time. The frequency of an oscillator will change with time because of structural fluctuations in the system, a process known as spectral diffusion. The FFCF is often sensitive to the different structural environments that a species interacts with over time, giving insight into the time scales of processes involved in spectral diffusion. For instance, bulk water undergoes fast local hydrogen bond fluctuations on a relatively fast, ∼0.4 ps, time scale and a set of slower processes on ∼1.7 ps time scale caused by complete randomization of the hydrogen bonding network.[11] In addition to extracting these time scales in the FFCF, 2D IR spectroscopy can also separate contributions of homogeneous (motionally narrowed) and inhomogeneous broadening to the line shape. Homogeneous broadening occurs when very fast fluctuations cause motional narrowing, while inhomogeneous broadening arises from slower processes. Water has a relatively large homogeneous component.[11] 2D IR spectroscopy has been extremely successful in understanding spectral diffusion in bulk water[6–8,12–15] and other hydrogen bonding systems,[11,16,17] protein and other biological systems,[18–26] as well as systems that undergo chemical exchange or isomerization.[27–32]

Through a time-ordered series of three input electric fields (ultrafast laser pulses), 2D IR spectroscopy can manipulate the quantum pathways by which a system evolves. The first pulse excites a coherent superposition of the ground (0) and first excited (1) vibrational states. After a time period τ, the evolution period, a second pulse interacts with the sample and brings the system into population states, 0 and 1. After a time period T_w, the waiting period, the third pulse interacts with the sample and creates another coherent superposition.

[a)]Electronic mail: fayer@stanford.edu.

The generated echo signal emits at a time $t \leq \tau$, which is the detection time period. A fourth beam, known as the local oscillator, is overlapped with the vibrational echo signal for heterodyned detection. In an experiment, τ is scanned at a series of fixed T_w values. The molecules undergo spectral diffusion during T_w due to dynamic structural evolution of the system. After Fourier transformation of the temporal interferograms obtained during the experiment, correlation spectra are obtained for the detection vs. initial excitation frequencies, referred to as ω_m (axis of echo emission, vertical axis) and ω_τ (axis of interaction with the first pulse, horizontal axis), respectively.

Various methods for extracting the FFCF from the 2D correlation spectra have been developed. A rigorous, and consequently more cumbersome, method involves choosing a trial function for the FFCF and using the nonlinear third order response functions to calculate 2D spectra. The FFCF parameters are iteratively adjusted until the calculated and experimental spectra agree.[3,4,33] This procedure becomes even more problematic when finite pulse durations must be taken into account. In addition, the quality of convergence of the fit is questionable, given that there are multiple adjustable parameters. The complexity surrounding the trial FFCF procedure has encouraged the development of simpler methods for extracting the FFCF.

2D IR observables such as the ellipticity,[34–37] eccentricity,[35] and dynamic line width[7,8] have all been used to extract dynamical information from 2D IR correlation spectra. Although these techniques are much simpler computationally compared to using a trial FFCF, these techniques are susceptible to distortions from finite pulse durations, sloping background absorption, Fourier filtering methods (such as apodization) as well as the overlap between the 0-1 and 1-2 transition peaks. The full FFCF, including a fast motionally narrowed (homogeneous) component, may be obtained via these methods, but a full treatment using nonlinear response theory must be used.

The center line slope (CLS) method has also been used to extract the FFCF from 2D IR measurements.[9,10] This method is particularly useful because the T_w-dependent portion of the FFCF may be obtained directly from the spectra without any response function calculations. The motionally narrowed component may be easily obtained using the CLS in conjunction with the linear IR absorption spectrum. In the CLS technique, slopes are calculated through the lines that connect the peak positions of one-dimensional cuts parallel to the ω_m axis for each correlation spectrum. This variant of the method is referred to as CLSω_m. When the cuts are taken parallel to the ω_τ axis, then the technique is called CLSω_τ. In CLSω_m, the slopes are plotted vs. T_w. In CLSω_τ, the inverse of the slopes vs. T_w are plotted. In either case, the CLS plot is equal to the normalized T_w-dependent portion of the FFCF. Figure 1 shows the CLS data for bulk water at two T_w's. The dotted lines are the peak positions through which the slope is calculated. In this work and in previous[23–25,38] studies, the CLSω_m technique is used because, unlike the CLSω_τ technique, it is not sensitive to distortions caused by the overlap of the 0-1 and 1-2 transitions. The CLSω_m technique, and the process by which the motionally narrowed component is obtained, will be discussed in more detail in Sec. II.

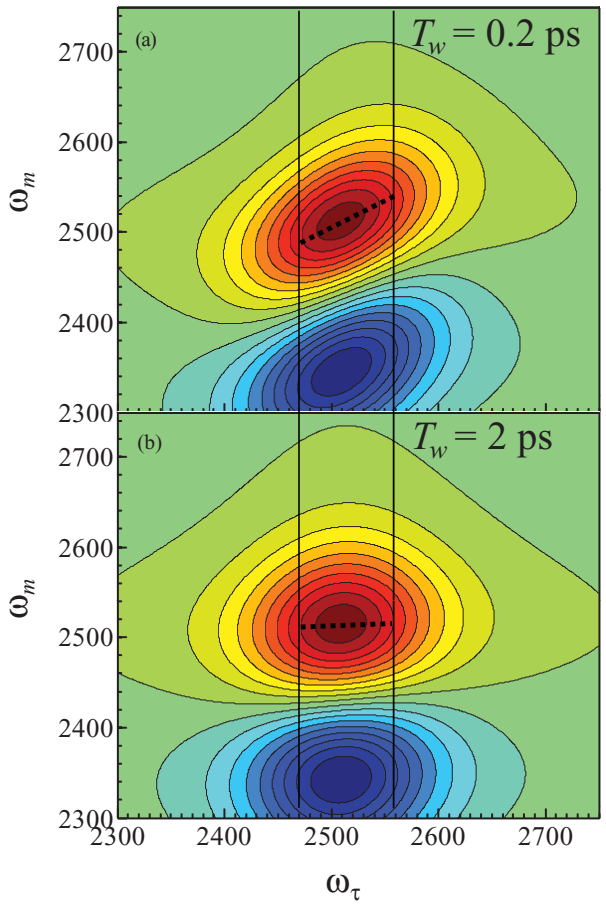

FIG. 1. Calculated 2D IR spectra for bulk water at $T_w = 0.2$ ps (a) and $T_w = 2$ ps (b). The solid lines show the direction of cuts through the spectra for the CLSω_m technique. The dotted lines show the peak positions for a series of cuts parallel to the ω_m axis (and the solid lines), also known as center line data. As T_w lengthens, the spectra become more symmetric, and the slope through the center line data approaches zero.

When a system is composed of a single vibrational component (such as the OD stretch of dilute HOD in bulk water), then analysis of the 2D IR spectra with the CLS method is relatively straightforward. Only one 0-1 peak is present in the spectrum, so the CLS cuts are taken at a range of frequencies around the 2D IR maximum value for each T_w. If a system has two separate components, and if the separation of peak transition frequencies for the components is large enough such that the system shows two distinct bands in the 2D IR spectrum, then the CLS analysis may be carried out on each band independently to yield the dynamics for each component. The question addressed in this paper is how one should treat a system of two components that are not spectrally resolved. In this scenario, the resulting spectrum only shows one 0-1 band, even though it is made up of two 0-1 bands, one from each component. 2D IR spectra are additive, so the overall observed spectrum can be thought of as the weighted average of two separate spectra. Each individual spectrum will in general have its own distinct dynamics, which CLS analysis should be able to determine, if the two components could be separated from one another. This paper will show that the

CLS results for the observed experimental spectra of a system with two components may be decomposed into contributions from each component, provided that the center line data of one of the components is known. The vibrational lifetimes, linear IR absorption spectra, and relative fractions of the components must also be known in order for the algorithm to work. It should be noted here that the term "component" in this work refers to a chemically distinct and separate vibrating species and not, for instance, a system of coupled oscillators on the same molecule. An example of a relevant system is water in reverse micelles. Over the years, experimentalists have used reverse micelles as model systems to probe the dynamics of water molecules in confined environments,[38–66] a topic that bears great significance to biological and industrial applications in which the behaviors of small amounts of water or water next to interfaces can severely impact the function of systems such as proteins, pharmaceuticals, and fuel cell membranes. In a reverse micelle, a water pool is surrounded by a shell of surfactant molecules that have hydrophilic head groups, which can either be charged or neutral. The surfactant molecules are suspended in a non-polar organic phase. A very popular surfactant for making reverse micelles is Aerosol-OT (AOT) because it makes monodispersed, spherical reverse micelles of easily tunable water pool diameters.[67–69] The size of the reverse micelle water pool is often denoted by the ratio of water to AOT, $w_0 = [H_2O]/[AOT]$.[69] Water pool diameters can range from 1.7 to 28 nm ($w_0 = 2$ to $w_0 = 60$). It has been shown that the population and orientational dynamics of water inside large AOT reverse micelles (diameters of 5.8 nm and greater) can be readily separated into bulk and interfacial components, each with distinct dynamics.[39,41] As of yet, there has been no analogous method presented to separate bulk and interfacial contributions to spectral diffusion. The extended CLS method presented in this paper can be applied not only to large reverse micelles which are composed of bulk and interfacial water environments but also to other two component systems that show only one band in their absorption and 2D IR spectra.

II. THEORETICAL DEVELOPMENT

A. CLS method for a single component system

The CLS method for systems of one component, or for systems with two spectrally resolved components, has been discussed in detail previously.[9,10] As explained in the introduction, the CLSω_m variant will be used in this work. In this technique, cuts through the 2D IR correlation plots are taken parallel to the ω_m axis and fit to Gaussian line shape functions to find the maximum at each frequency. Typically, the cuts are taken at a range of ω_τ frequencies surrounding the location of the maximum of the 2D spectrum. The set of peaks and corresponding ω_τ frequencies are referred to as center line data. The CLSω_m is not sensitive to the overlap between the 0-1 and 1-2 bands, allowing cuts to be taken on either side of the spectral maximum even if there is overlap of the 0-1 and 1-2 bands. The peak positions of the Gaussian line shape fits are plotted vs. their corresponding ω_τ frequencies, and the slope of the resulting line is calculated. This process is repeated for each T_w, and a plot of slopes vs. T_w is obtained. The CLS plot corresponds to the T_w-dependent portion of the normalized FFCF. Figures 1(a) and 1(b) show calculated 2D IR spectra for bulk water at $T_w = 0.2$ ps and 2 ps based on its known FFCF.[11] The CLS method assumes Gaussian fluctuations,[9,10] an assumption that does not strictly apply for water systems.[70,71] For the model calculations presented here, the assumption of Gaussian fluctuations for water does not affect the results. The CLS is a valid experimental observable whether the fluctuations are Gaussian or not. The center line data of ω_m peak positions at each T_w are indicated by the dotted lines. The direction of the cuts is denoted by the solid lines. Typically, the center line data are found over a limited range of frequencies around the maximum in the 2D IR spectrum. For water systems, a typical range is ± 30–40 cm^{-1} about the maximum. Figure 2 shows the CLS decay for the bulk water system. The data points in Figure 2 are the slopes calculated from the center line data of the 2D spectra at each T_w. A large homogeneous component results in the CLS having an initial value well below 1.

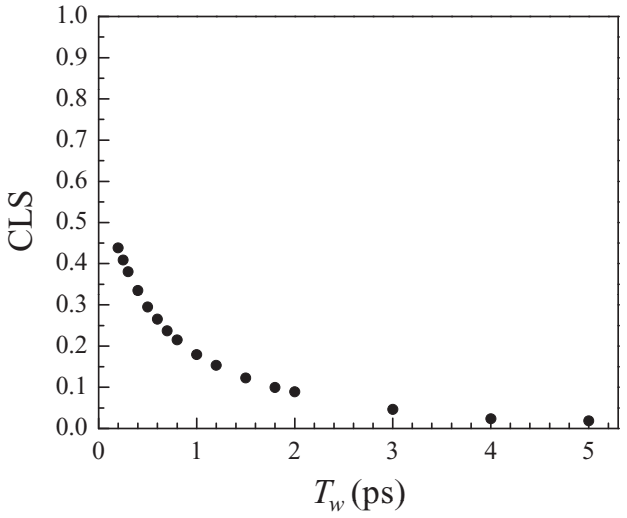

FIG. 2. CLS decay curve for bulk water. Spectral diffusion is relatively rapid and has mostly decayed by ~2 ps. There is a large homogeneous component, as seen by the large drop from 1 of the data.

The FFCF is composed of homogeneous (motionally narrowed) and inhomogeneous components. Using a sum of exponentials, the FFCF is

$$C_1(t) = \langle \delta\omega_{10}(t)\delta\omega_{10}(0)\rangle = \frac{\delta(t)}{T_2} + \sum_i \Delta_i^2 e^{-t/\tau_i}, \qquad (1)$$

where $\langle \delta\omega_{10}(t)\delta\omega_{10}(0)\rangle$is the correlation function for the fluctuating 0-1 transition frequency, and $\delta\omega(t) = \langle\omega\rangle - \omega(t)$. The T_2 parameter is the dephasing time given by

$$\frac{1}{T_2} = \frac{1}{T_2^*} + \frac{1}{2T_1} + \frac{1}{3\tau_{or}}, \qquad (2)$$

where T_2^* is the pure dephasing time, T_1 is the vibrational lifetime, and τ_{or} is the orientational relaxation time constant. The delta function term that involves the dephasing time in Eq. (1) is the motionally narrowed component. The Δ_i terms are frequency fluctuation amplitudes, and the τ_i terms are their associated time constants. The time constants represent different

time scales for processes that contribute to spectral diffusion. The magnitude of a Δ_i term represents the contribution to the line shape of processes occurring on each time scale.

CLS data are often fit to a multiexponential decay, yielding a set of time constants and associated amplitudes. The parameters obtained from the CLS data like that shown in Figure 2 are used in the overall calculation that determines the motionally narrowed component, yielding the full FFCF.[9] The values of the time constants are accurate, as well as the amplitude corresponding to the longer of the time constants. Due to the short time approximation,[9,34,72] the amplitude of the first component can be pushed into the homogeneous contribution. Therefore, the CLS method cannot accurately determine the exact amplitudes of the fast inhomogeneous component and the homogeneous component. To determine these, the absorption line shape is employed. The absorption spectrum is the Fourier transform of the linear response function, $R_1(t)$,

$$R^1(t) = |\mu_{10}|^2 \, e^{-i\langle\omega_{10}\rangle t} e^{-ig_1(t)}, \tag{3}$$

where μ_{10} is the transition dipole moment of the 0-1 transition, $\langle\omega_{10}\rangle$ is the average 0-1 transition frequency, and g_1 is the line shape function given by

$$g_1(t) = \int_0^t d\tau_2 \int_0^{\tau_2} d\tau_1 \, \langle\delta\omega_{10}(t)\delta\omega_{10}(0)\rangle. \tag{4}$$

Equation (4) shows the link between the absorption spectrum and the FFCF. Using the amplitude of the fast inhomogeneous decay and the homogeneous component as the only adjustable parameters, the absorption line shape of the system is fit simultaneously with the CLS decay.[9,11,38] This procedure is able to accurately determine the motionally narrowed component as well as the amplitude of the first inhomogeneous component.

B. Extension of the CLS method to two components

Following the work of Kwak *et al.*,[10] the 2D IR line shape function may be expressed as

$$R(\omega_m, \omega_\tau) = \frac{4\pi\sqrt{2}}{K(T_w)^{1/2}} \exp\left(\frac{A(\omega_m, \omega_\tau)}{K(T_w)}\right) - \frac{2\pi s^2\sqrt{2}}{Q(T_w)^{1/2}} \times \exp\left(\frac{B(\omega_m, \omega_\tau)}{Q(T_w)}\right). \tag{5}$$

In this expression, $s = \mu_{21}/\mu_{10}$, the ratio of transition dipole moments for the 1-2 and 0-1 transitions. The remaining parameters are as follows:

$$\begin{aligned} A(\omega_m, \omega_\tau) &= -\left(C_1(0)\omega_m^2 - 2C_1(T_w)\omega_m\omega_\tau + C_1(0)\omega_\tau^2\right), \\ B(\omega_m, \omega_\tau) &= -\left(C_1(0)(\omega_m + \Delta)^2 - 2C_2(T_w)(\omega_m + \Delta)\omega_\tau \right. \\ &\quad \left. + C_3(0)\omega_\tau^2\right), \\ K(T_w) &= \sqrt{C_1(0)^2 - C_1(T_w)^2}, \\ Q(T_w) &= \sqrt{C_1(0)C_3(0) - C_2(T_w)^2}, \end{aligned} \tag{6}$$

where the Δ term is the anharmonic frequency shift of the 0-1 and 1-2 transitions and

$$\begin{aligned} C_1(t) &= \langle\delta\omega_{10}(\tau_1)\delta\omega_{10}(0)\rangle, \\ C_2(t) &= \langle\delta\omega_{21}(\tau_1)\delta\omega_{10}(0)\rangle, \\ C_3(t) &= \langle\delta\omega_{21}(\tau_1)\delta\omega_{21}(0)\rangle. \end{aligned} \tag{7}$$

The CLSω_m technique finds the maximum value of the line shape function along a slice taken parallel to the ω_m axis. In other words, the derivative of Eq. (5) with respect to ω_m is set to 0 according to

$$\frac{\partial R(\omega_m, \omega_\tau)}{\partial\omega_m} = 0 = \frac{4\pi\sqrt{2}}{K(T_w)^{3/2}} \exp\left(\frac{A(\omega_m, \omega_\tau)}{K(T_w)}\right) \frac{\partial A}{\partial\omega_m} - \frac{2\pi s^2\sqrt{2}}{Q(T_w)^{3/2}} \exp\left(\frac{B(\omega_m, \omega_\tau)}{Q(T_w)}\right) \frac{\partial B}{\partial\omega_m}. \tag{8}$$

After some rearrangement of Eq. (8), a set of ω_m and ω_τ that correspond to a maximum in the slice parallel to ω_m is defined by

$$\frac{2Q(T_w)^{3/2}}{s^2K(T_w)^{3/2}} \exp\left(\frac{A(\omega_m, \omega_\tau)}{K(T_w)} - \frac{B(\omega_m, \omega_\tau)}{Q(T_w)}\right) = \frac{-2C_1(0)(\omega_m + \Delta) + 2C_2(T_w)\omega_\tau}{-2C_1(0)\omega_m + 2C_1(T_w)\omega_\tau}. \tag{9}$$

As shown by Kwak *et al.*[10] the slope through the set of points described by Eq. (9) may be found by finding the total derivative of Eq. (9) with respect to ω_τ and then solving for $\frac{d\omega_m}{d\omega_\tau}$. After simplification it is found that,

$$\frac{d\omega_m}{d\omega_\tau} = \frac{\dfrac{C_1(0)(C_1(T_w) - C_2(T_w))\omega_\tau + C_1(0)C_1(T_w)\Delta}{(C_1(T_w)\omega_\tau - C_1(0)\omega_m)^2} - D(\omega_\tau, \omega_m, T_w, s)\left[\dfrac{C_1(T_w)\omega_m - C_1(0)\omega_\tau}{\sqrt{C_1(0)^2 - C_1(T_w)^2}} - \dfrac{C_2(T_w)(\omega_m + \Delta) - C_3(0)\omega_\tau}{\sqrt{C_1(0)C_3(0) - C_2(T_w)^2}}\right]}{\dfrac{C_1(0)(C_1(T_w) - C_2(T_w))\omega_m + C_1(0)^2\Delta}{(C_1(T_w)\omega_\tau - C_1(0)\omega_m)^2} + D(\omega_\tau, \omega_m, T_w, s)\left[\dfrac{C_1(T_w)\omega_\tau - C_1(0)\omega_\tau}{\sqrt{C_1(0)^2 - C_1(T_w)^2}} - \dfrac{C_2(T_w)\omega_\tau - C_3(0)(\omega_m + \Delta)}{\sqrt{C_1(0)C_3(0) - C_2(T_w)^2}}\right]}, \tag{10}$$

where

$$D(\omega_\tau, \omega_m, T_w, s) = \left(\frac{2(C_1(0)C_3(0) - C_2(T_w)^2}{s^2C_1(0)^2 - C_1(T_w)^2}\right) \times \exp\left(-\frac{C_1(0)\omega_m^2 - 2C_1(T_w)\omega_m\omega_\tau + C_1(0)\omega_\tau^2}{2\sqrt{C_1(0)^2 - C_1(T_w)^2}} + \frac{C_1(0)(\omega_m+\Delta)^2 - 2C_2(T_w)(\omega_m+\Delta)\omega_\tau + C_3(0)\omega_\tau^2}{2\sqrt{C_1(0)C_3(0) - C_2(T_w)^2}}\right). \quad (11)$$

Within the harmonic approximation for a three level vibrational system, all of the correlation functions are equal to each other. In this situation, $C(t) = C_1(t) = C_2(t) = C_3(t)$ and the slope (Eq. (10)) becomes the normalized FFCF,[10]

$$\frac{d\omega_m}{d\omega_\tau} = \frac{C(T_w)}{C(0)}. \quad (12)$$

When two species are involved, the 2D IR line shape becomes

$$R(\omega_m, \omega_\tau) = f_1(\omega_\tau, T_w)\left[\frac{4\pi\sqrt{2}}{K_1(T_w)^{1/2}}\exp\left(\frac{A_1(\omega_m, \omega_\tau)}{K_1(T_w)}\right) - \frac{2\pi s^2\sqrt{2}}{Q_1(T_w)^{1/2}}\exp\left(\frac{B_1(\omega_m, \omega_\tau)}{Q_1(T_w)}\right)\right] + (1 - f_1(\omega_\tau, T_w))\left[\frac{4\pi\sqrt{2}}{K_2(T_w)^{1/2}}\exp\left(\frac{A_2(\omega_m, \omega_\tau)}{K_2(T_w)}\right) - \frac{2\pi s^2\sqrt{2}}{Q_2(T_w)^{1/2}}\exp\left(\frac{B_2(\omega_m, \omega_\tau)}{Q_2(T_w)}\right)\right], \quad (13)$$

where the A_i, B_i, K_i, and Q_i parameters are defined in a similar manner as given above (Eq. (6)) but correspond to different components with different sets of correlation functions (Eq. (7)). The f_1 term corresponds to a frequency and T_w-dependent fraction term. The fraction reflects the overall concentration of a species at a certain wavelength.

In two component systems such as reverse micelles, the fraction can be obtained from infrared spectral analysis.[39,41,49] As a concrete example for calculating the fraction term, the 2D IR spectrum of a large AOT reverse micelle will be used as a model, but the AOT system will not be used to test the modified CLS method developed here. Instead, hypothetical systems are constructed. As discussed in the introduction, the water nanopool in a large AOT reverse micelle consists of a bulk water core and water at the AOT interface. Each spectrum may be thought of as a linear combination of the bulk water spectrum and the spectrum of $w_0 = 2$, a very small reverse micelle. In the $w_0 = 2$ system, essentially all of the waters interact with surfactant head groups. Thus, the spectra are decomposed into "core" and "shell" spectra.[49]

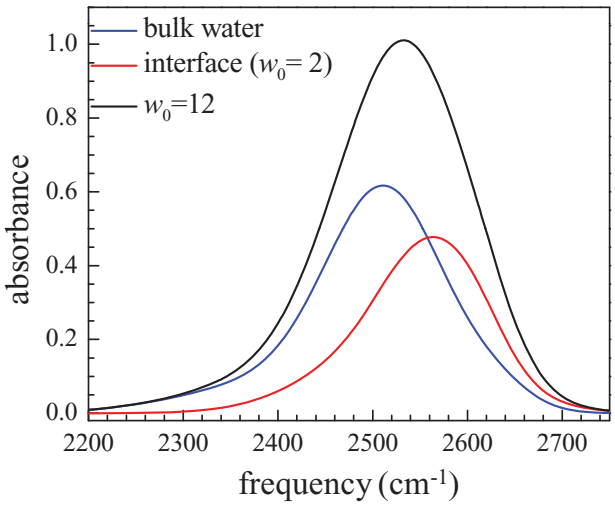

FIG. 3. Linear IR absorption spectra for water (5% HOD in H_2O) inside the AOT $w_0 = 12$ reverse micelle (black line). The overall spectrum may be decomposed into a linear combination of the bulk water (5% HOD in H_2O) spectrum (blue line) and the $w_0 = 2$ spectrum (red line) in which all waters interact with the surfactant head group interface.

Figure 3 shows the component core and shell spectra for water in the $w_0 = 12$ AOT reverse micelle. It should be noted that the water measured inside the reverse micelle is the OD stretch of 5% HOD in H_2O. Dilute HOD in H_2O is used in experiments to eliminate vibrational excitation transfer and so that there is a single local stretching mode.[73,74] The model calculations performed in this work use the OD stretch of HOD in H_2O.

The overall linear absorption spectrum of a two component system takes the following form:

$$I_{tot}(\omega_\tau) = a_1 I_1(\omega_\tau) + (1 - a_1)I_2(\omega_\tau) = S_1(\omega_\tau) + S_2(\omega_\tau), \quad (14)$$

where $I_i(\omega_\tau)$ are the component spectra, and a_1 is a single weighting factor. For $w_0 = 12$, $a_1 = 0.56$.

Each ω_τ will yield a different fraction of component i determined by the overlap of the infrared spectra of the two components. The relative populations at a particular time, T_w, are also dependent on the vibrational lifetimes. Each component spectrum of the 2D correlation plot will decrease in amplitude at a rate defined by its vibrational lifetime. The f_1 term can be calculated by

$$f_1(\omega_\tau, T_w) = \frac{S_1(\omega_\tau)e^{-T_w/T_1^1}}{S_1(\omega_\tau)e^{-T_w/T_1^1} + S_2(\omega_\tau)e^{-T_w/T_1^2}}, \quad (15)$$

where the S_i terms are the infrared spectra of components 1 and 2 defined in Eq. (14), and the T_1^i are their associated vibrational lifetimes. Figure 4 illustrates the behavior of Eq. (15) with changing wavelength and T_w for the AOT $w_0 = 12$ system. Often in two component systems the vibrational lifetimes for each component remain invariant with wavelength. Only the fractional populations of each component change with wavelength. If the vibrational lifetime is wavelength-dependent, then the known lifetimes could be incorporated into Eq. (15) at the corresponding wavelengths.

Similar to the above derivation, the location of the maximum of a slice along the ω_m axis is found by setting the partial derivative of Eq. (13) with respect to ω_m to 0,

$$\frac{\partial R(\omega_m,\omega_\tau)}{\partial \omega_m} = f_1(\omega_\tau,T_w)_1\left[\frac{4\pi\sqrt{2}}{K_1(T_w)^{3/2}}\exp\left(\frac{A_1(\omega_m,\omega_\tau)}{K_1(T_w)}\right)\frac{\partial A_1(\omega_m,\omega_\tau)}{\partial\omega_m} - \frac{2\pi s^2\sqrt{2}}{Q_1(T_w)^{3/2}}\exp\left(\frac{B_1(\omega_m,\omega_\tau)}{Q_1(T_w)}\right)\frac{\partial B_1(\omega_m,\omega_\tau)}{\partial\omega_m}\right] + (1-f_1(\omega_\tau,T_w))\left[\frac{4\pi\sqrt{2}}{K_2(T_w)^{3/2}}\exp\left(\frac{A_2(\omega_m,\omega_\tau)}{K_2(T_w)}\right)\frac{\partial A_2(\omega_m,\omega_\tau)}{\partial\omega_m} - \frac{2\pi s^2\sqrt{2}}{Q_2(T_w)^{3/2}}\exp\left(\frac{B_2(\omega_m,\omega_\tau)}{Q_2(T_w)}\right)\frac{\partial B_2(\omega_m,\omega_\tau)}{\partial\omega_m}\right] = 0. \quad (16)$$

Again, Eq. (16) defines a set of ω_m and ω_τ values that correspond to the location of the maximum along a slice parallel to ω_m. As before, we may take the derivative of Eq. (16) with respect to ω_τ to obtain an equation for the slope of the curve created by the maxima locations. Even after extensive rearrangement and using the harmonic approximation for each set of correlation functions associated with a given component, a complicated expression for $\frac{d\omega_m}{d\omega_\tau}$ is obtained. The full form and derivation of $\frac{d\omega_m}{d\omega_\tau}$ are presented in the Appendix.

It is discovered that the slope, $\frac{d\omega_m}{d\omega_\tau}$, does not yield the normalized FFCF, in contrast to the case for a single ensemble. An expression involving the center line positions, the fractions, and their derivatives is obtained, showing that the slope in this two component situation is not a weighted average of the individual normalized FFCFs. Instead, we find that the center line data are a weighted average of the center line data for each component. If a center line point corresponding to a maximum along ω_m is denoted as ω_m^*, then this relationship may be mathematically expressed by

$$\omega_{mC}^*(\omega_m,\omega_\tau,T_w) = f_1(\omega_\tau,T_w)\omega_{m1}^*(\omega_m,\omega_\tau,T_w) + (1-f_1(\omega_\tau,T_w))\omega_{m2}^*(\omega_m,\omega_\tau,T_w), \quad (17)$$

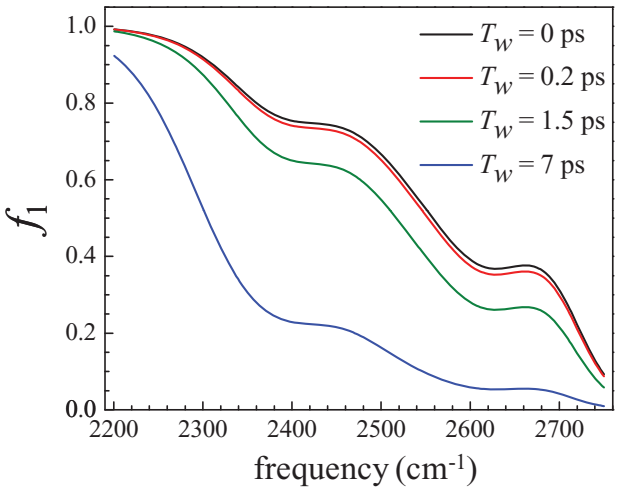

FIG. 4. Frequency and T_w-dependent fraction of bulk water for the AOT w_0 = 12 reverse micelle system.

where ω_{mC}^*, ω_{m1}^*, and ω_{m2}^* represent the sets of center line data for the experimentally observed two component system, component 1 by itself, and component 2 by itself, respectively. If one of the components can be measured or simulated independently from the two component system, then the second component may be obtained from simple rearrangement of Eq. (17),

$$\omega_{m2}^*(\omega_m,\omega_\tau,T_w) = \frac{(\omega_{m2C}^*(\omega_m,\omega_\tau,T_w) - f_1(\omega_\tau,T_w)\omega_{m1}^*(\omega_m,\omega_\tau,T_w))}{(1-f_1(\omega_\tau,T_w))}, \quad (18)$$

provided that the linear spectra and the fraction term are also known (see Appendix). Equation (18) provides a simple and experimentally tractable expression for back-calculating the center line data for the second component from known quantities. The center line data for component 2 may be back-calculated for T_w's common to both the combined system and the first component. From the resulting component 2 center line data, the CLS values (slopes) may be determined and plotted vs. T_w, from which the FFCF parameters can be extracted according to the procedures outlined in Sec. II A, effectively isolating the dynamics of component 2 from component 1. Section III will test this algorithm for a variety of cases.

C. Model calculation details

The two component CLS method was tested using sets of model cases in which two different FFCF functions are formulated separately. For our purposes we chose one of the FFCFs to be the FFCF for bulk water (Table I, system 1). In all cases studied here, component 2 corresponds to a hypothetical FFCF. The FFCF parameters are inserted into the third order response functions that describe the emitted 2D IR signal electric field.[3,75,76] The response functions are used to construct 2D correlation plots on which CLS analysis may be performed. In addition to the FFCF parameters, a center frequency, anharmonicity, and vibrational lifetime are also required to calculate the 2D spectra. When generating spectra for a system with two components (known as the combined system), the sets of response functions for each com-

TABLE I. First model case FFCF parameters.

System	Γ (cm^{-1})	Δ_1 (cm^{-1})	t_1 (ps)	Δ_2 (cm^{-1})	t_2 (ps)	ω_0 (cm^{-1})	a_1	T_1 (ps)
1	76	41	0.38	34	1.7	2509	0.5	1.8
2	40	45	0.9	30	5	variable	0.5	4.5

ponent are weighted by a fractional concentration (a_1 from Eq. (14)). Calculated 2D spectra may be independently obtained for each component by itself as well as the combined system. The FFCF of component 2 can be back-calculated using the method outlined above, and then the procedure can be verified since the actual starting FFCF parameters of component 2 are known.

It should be noted that to apply Eq. (18) to a two component system in an experimental situation, none of the individual FFCFs actually need to be known. The only required information is the set of center line data for one of the components and the experimentally measured system (plus the vibrational lifetime and other details). Here we examine model cases and begin by knowing the FFCFs of both components so that the efficacy of the algorithm may be evaluated.

III. TESTING THE TWO COMPONENT CLS METHOD

A. Practical application of the two component CLS algorithm

The flow chart in Figure 5 illustrates the chain of events for back-calculating the FFCF of component 2 using calculated 2D IR and linear IR data. The algorithm is easily adaptable to experimental data as long as 2D and linear IR spectra for the combined system and for one of the components can be measured independently. Again, in an experimental situation it is not actually necessary to know the FFCF of component 1; only the center line data are required. Each block in Figure 5 is referenced with a letter so that the reader can follow along with the description presented in this section. In the first step (*a*), the required pieces of information are collected. FFCF parameters are chosen for each component (the bulk water FFCF parameters are used for component 1 while component 2 is hypothetical). In addition, the center frequencies, vibrational lifetimes, and the anharmonicity values between the 0-1 and 1-2 transitions must also be known. Reasonable values were chosen for the second component. The last piece of required information is the fractional concentration of species used to weight the linear and 2D IR spectra (a_1 from Eq. (14)). The starting information is used to calculate the linear absorption spectra of the components that make up the combined system spectrum, according to Eq. (14), as well as center line data for components 1 and 2 separately and the combined system (*b*). From the linear absorption spectra, the f_1 fraction terms may then be calculated using Eq. (15) and the vibrational lifetimes of the two components (*c*). The center line data calculated from the 2D spectra for component 1 and the combined system are used in Eq. (18) to back-calculate the center line data for component 2 (*c*). Figure 6 shows representative results for the center line back-calculation. The black circles

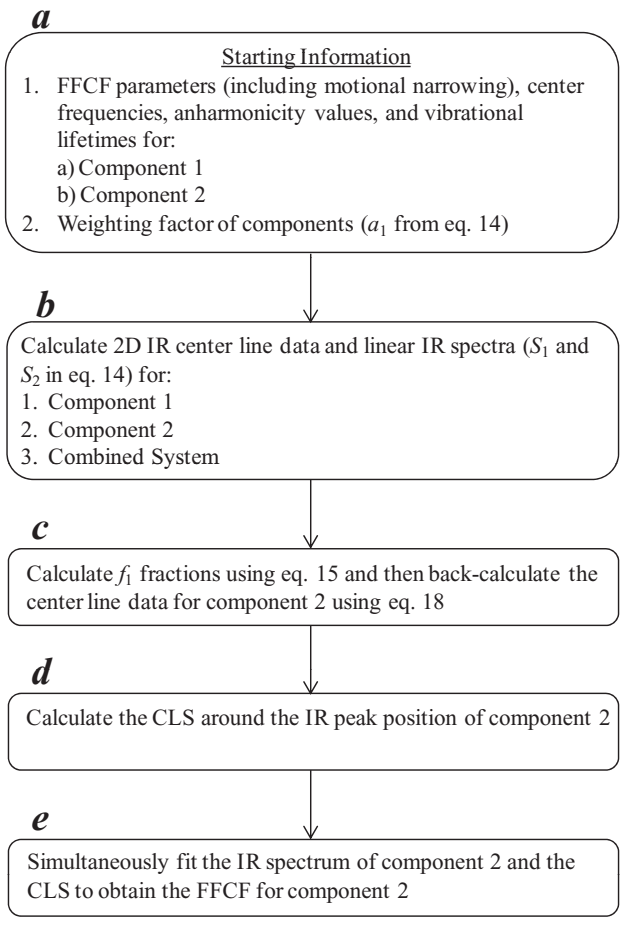

FIG. 5. Flow chart illustrating the algorithm that back-calculates the center line data and FFCF for a second component from known information (Eq. (18)). Because the model systems are calculated from known FFCF parameters, the accuracy of the algorithm may be easily verified.

are the center line data from the calculated 2D IR spectrum of the model combined system. The blue circles are the center line for component 1 by itself. The green circles are the back-calculated center line for component 2 by itself using Eq. (18). The red line that passes through the black circles is the reconstructed center line data for the combined system obtained by combining the back-calculated component 2 center line and the known component 1 center line with the correct fraction terms. The red line exactly reproduces the data represented by the black circles, showing the virtually quantitative agreement of the calculation.

The back-calculated center line data for component 2 is then subjected to CLS analysis (*d*). The CLS data are determined for a ~30–40 cm^{-1} range around the center frequency of component 2 (one of the pieces of starting information). For spectra with smaller bandwidths, a smaller range should be chosen. The CLS is then simultaneously fit with the IR spectrum of component 2 (step *b*) in order to obtain the FFCF (*e*).

B. Non-overlapping bands

In some systems, the constituent components yield spectrally resolved line shapes. For example, the red and blue

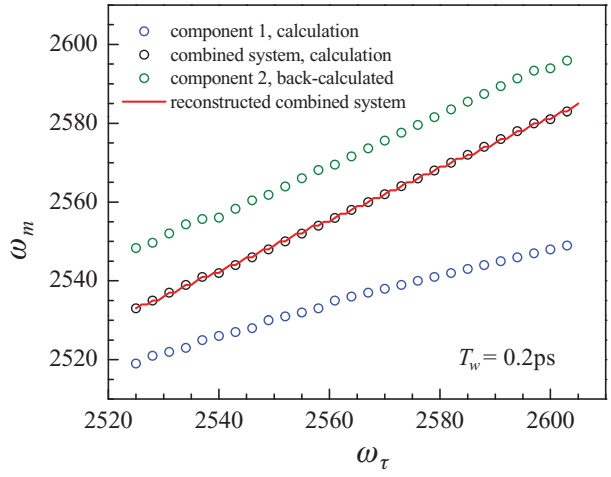

FIG. 6. Representative center line data used in the algorithm. The known center line data for bulk water are the blue circles, while the center line data for the known combined system are shown by the black circles. After applying the algorithm, the center line data for component 2 are produced (green circles). The calculated center line data can then be recombined with the known bulk water data to reproduce the known combined data (red line).

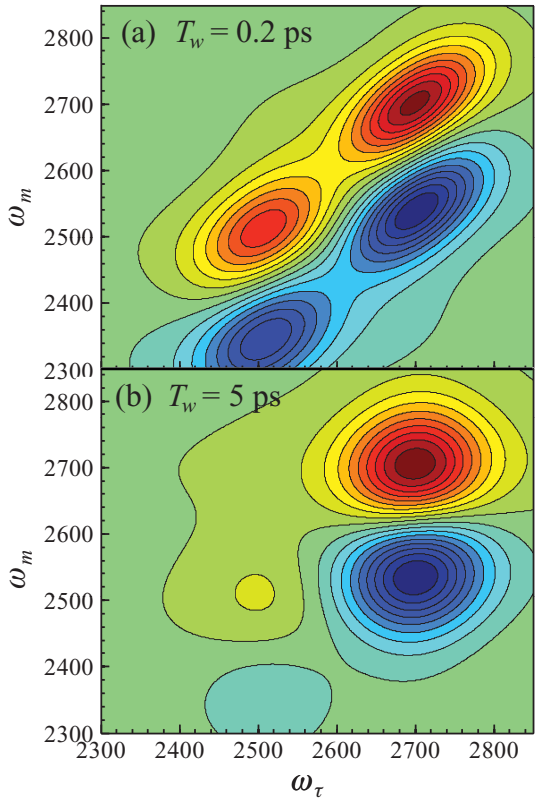

FIG. 7. Calculated 2D IR spectra for non-overlapping bands at $T_w = 0.2$ ps (A) and $T_w = 5$ ps (B). The bulk water system is the set of peaks on the left side of the spectra (lower frequency). Because the two components have different vibrational lifetimes, the spectra decay at different rates.

states of the CO stretching mode of horseradish peroxidase (HRP) give rise to narrow peaks at 1903.7 cm^{-1} and 1932.7 cm^{-1}, respectively.[35] The bandwidths of these peaks are 10 and 15 cm^{-1}, so the peaks are readily distinguishable. In this situation, CLS analysis is performed independently on each peak to obtain the individual FFCFs.[9] It will be seen shortly that the model cases tested in this study involve a bulk water-like component which has a much broader absorption spectrum compared to the HRP system. We would like to stress that the modified CLS analysis and relevant discussions presented here can apply to many two component systems and not just those with water.

Table I lists FFCF parameters that were used to construct a series of calculated spectra for testing the two component CLS method. The set of FFCF parameters in Table I is collectively referred to as the first model case, but it is used to generate four separate situations involving different component 2 center frequencies. The first row contains the known FFCF parameters for bulk water[11] as well as the center frequency (2509 cm^{-1}) and the vibrational lifetime, T_1. Each concentration (a_1) was set to a fraction of 0.5. The only parameter varied in each scenario is the center frequency (ω_0) for the second component. In the non-overlapping case discussed in this section, the center frequency of component 2 was set to 2700 cm^{-1}. Figure 7 displays calculated 2D IR spectra for this system at $T_w = 0.2$ and 5 ps. The 0-1 and 1-2 bands due to bulk water (component 1) are located on the red side of the plot and by 5 ps are almost completely depleted due to a faster vibrational lifetime. T_1 for component 2 is 4.5 ps, while T_1 for bulk water is 1.8 ps.[39] Spectra were also calculated separately for component 1 and component 2. If CLS analysis is performed on the individual bands of the combined spectra shown in Figure 7, then the resulting CLS curves essentially match the CLS curves calculated for the separate sets of spectra for bulk water and component 2. Figure 8 shows the excellent agreement of these CLS calculations. There is no need to apply the algorithm presented in Figure 5. Since the peaks basically have no overlap, it is not surprising that the CLS for each peak can be readily extracted.

C. Overlapping but distinguishable bands

Figure 9(a) shows a 2D IR spectrum for the combined system (Table I) with the center of the second component set to 2650 cm^{-1}. In this situation, two bands can be distinguished, but there is significant overlap between them. Despite this overlap, the CLS can still be calculated separately from the individual peaks. The accuracy is improved if the CLS is calculated slightly more to the blue of the center for component 2 and more to the red of the center for component 1. Figure 9(b) shows the CLS results for component 2. The red circles are the CLS calculated from the 2D IR spectra [Figure 9(a)] between 2650 and 2730 cm^{-1}. The green circles are the CLS calculated from single 2D IR spectra of component 2 by itself. The black circles are the CLS from the center line data back-calculated using Eq. (18). Again, there is excellent agreement between the data sets. The important result here is that the CLS can be obtained accurately from each band individually even though there is substantial overlap. In this case, it is not necessary to know the parameters for component 1. The CLS curves of both component 1 and component 2 can be obtained.

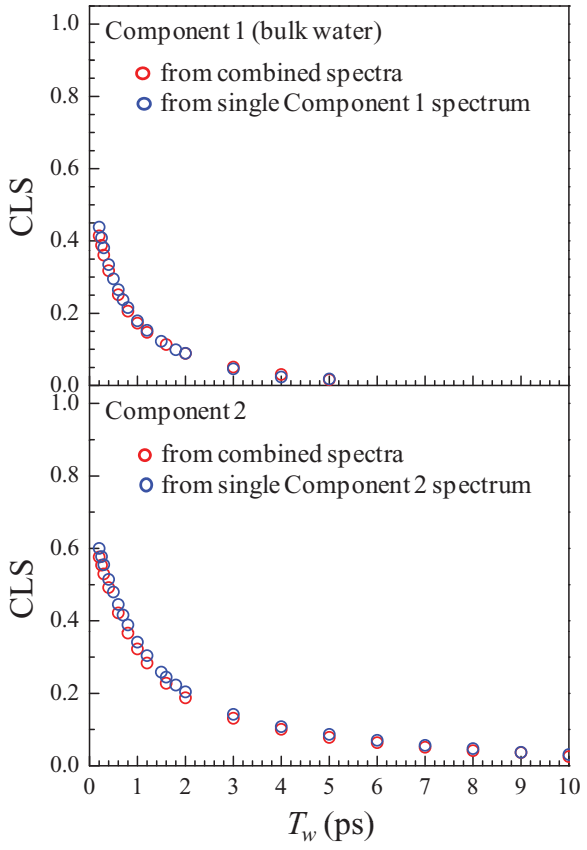

FIG. 8. Model case 1 for non-overlapping bands (centers of 2509 and 2700 cm^{-1}): CLS decay curves for bulk water (a) and component 2 (b). The red dots are the CLS calculations performed on the spectra when both components are present, while the blue dots denote the CLS calculated on the simulated bulk water and component 2 systems by themselves. Because the peaks are well-separated, the CLS results for each component (blue vs. red) match almost perfectly.

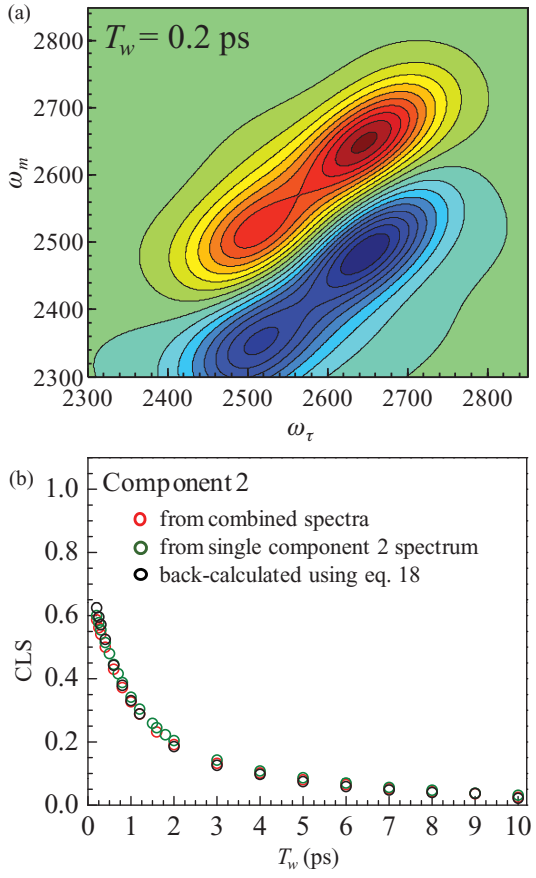

FIG. 9. Model case 1 for overlapped but distinguishable bands (centers of 2509 and 2650 cm^{-1}): Calculated 2D IR spectrum at T_w = 0.2 ps (a) and the CLS results for the system (b). The red dots are the CLS calculated for component 2 from the combined system 2D IR spectra. The green dots are the CLS curve obtained from the calculated 2D spectra of component 2 by itself. The black dots are the CLS for component 2 after applying Eq. (18).

D. Unresolved overlapping bands

Figure 10(a) shows a 2D IR spectrum when the center of component 2 (Table I) is set to 2600 cm^{-1}. The central lobe is quite elongated, but there is no clear separation into two bands. Figure 11(a) corresponds to the case where the center of component 2 (Table I) is 2550 cm^{-1} and resembles a spectrum that might arise from a single component. The two peaks are so overlapped that there is no indication that there are two components. In such a situation, it is necessary to know whether two species contribute. In these strongly overlapping cases, Eq. (18) can be used to obtain the CLS for component 2. The results for these two cases [Figures 10(a) and 11(a)] are presented in Figures 10(b) and 11(b). The green circles are the calculated CLS from the single component 2 spectra without component 1. The black circles are the results from applying Eq. (18). The results from Eq. (18) (black circles) differ slightly from the component 2 simulation results (green circles). Table II lists the FFCF parameters obtained from simultaneously fitting the CLS curves resulting from Eq. (18) and the FT IR spectra of component 2 at the two center positions (2600 and 2550 cm^{-1}). Because the curves do not exactly agree, there is some error in the magnitude of the homogeneous component, but the remaining parameters (Δ's and time constants) have excellent agreement with the starting parameters for the model case listed in Table I. Given that the two bands are completely indistinguishable in either the linear IR spectrum or in the 2D IR spectra, the accuracy of the extracted component 2 parameters demonstrates the usefulness of the method.

In verifying the method, many model calculations with various input parameters were used. These all gave good agreement between the extracted component 2 FFCF parameters and the component 2 FFCF parameters used in the calculations. Table III illustrates a different model system with two components, collectively referred to as the second model case. Component 1 is the same as in Table I, but the second component consists of a homogeneous component, an exponential decay, and a static offset (Δ_s) as given in Table III. The resulting 2D IR spectra are so close together that the spectrum

TABLE II. FFCF parameters obtained for component 2 via Eq. (18) and simultaneous fitting.

Component 2 center	Γ (cm^{-1})	Δ_1 (cm^{-1})	t_1 (ps)	Δ_2 (cm^{-1})	t_2 (ps)
2600 (cm^{-1})	47	49	0.8	27	5.1
2550 (cm^{-1})	45	46	0.9	29	4.9

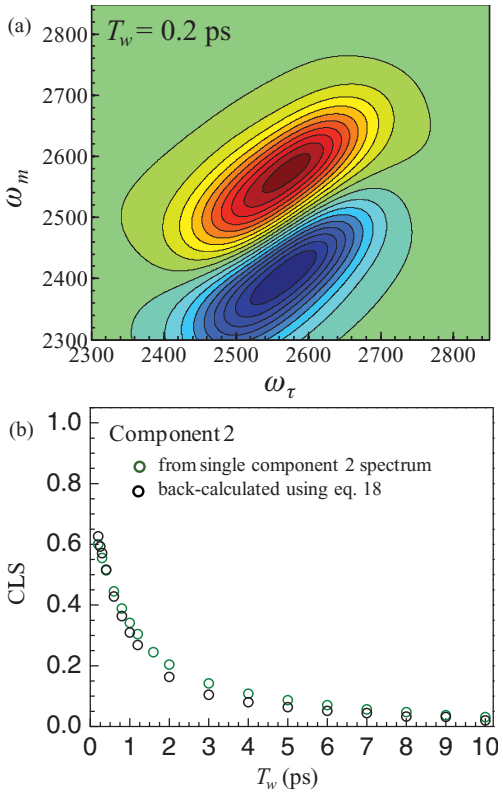

FIG. 10. Model case 1 for overlapping bands (centers of 2509 and 2600 cm^{-1}): Calculated 2D IR spectrum at T_w = 0.2 ps (a) and the CLS results for the system (b). The green dots are the CLS from the calculated 2D spectra of component 2 by itself. The black dots are the component 2 results after applying Eq. (18).

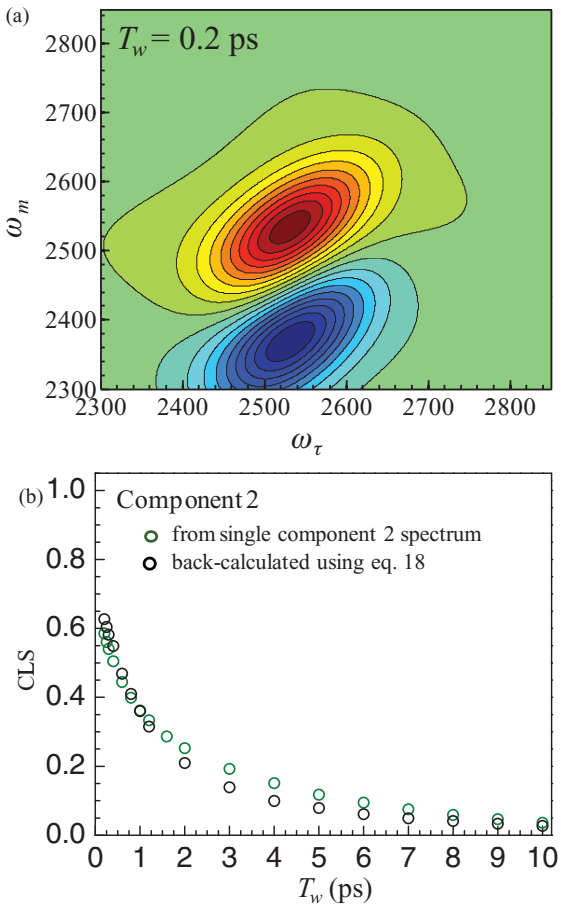

FIG. 11. Model case 1 for overlapping bands (centers of 2509 and 2550 cm^{-1}): Calculated 2D IR spectrum at T_w = 0.2 ps (a) and the CLS results for the system (b). The green dots are the CLS from the calculated 2D spectra of component 2 by itself. The black dots are the component 2 results after applying Eq. (18).

consists of a single 0-1 peak, just as in the other model cases in this section. Figure 12 shows that the CLS calculation using only the component 2 spectra and the back-calculation of the CLS using Eq. (18) have some error. However, simultaneously fitting with the CLS and IR spectrum recovers the homogeneous component quite accurately. The FFCF parameters obtained from the Eq. (18) CLS results are listed in the third row of Table III. The agreement is essentially quantitative.

One interesting question is what happens when the CLS is calculated around the 2D IR centers of the spectra of the combined system, without decomposing the dynamics into two components? Figure 13 shows the CLS decay for the first model case (Table I) with center frequencies of 2509 and 2550 cm^{-1}. Each CLS data point was calculated for ±40 cm^{-1} around the peak position of the corresponding spectrum. Because there are two components that decay with different vibrational lifetimes, the center steadily shifts from ~2530 cm^{-1} at T_w = 0.2 ps to 2550 cm^{-1} at T_w = 10 ps. When the curve in Figure 13 is fit with a biexponential decay, the fit parameters are a_1 = 0.30, t_1 = 0.6 ps, a_2 = 0.39, t_2 = 4.3 ps, where the a_i and t_i terms are amplitudes and de-

TABLE III. Second model case parameters.

System	Γ (cm^{-1})	Δ_1 (cm^{-1})	t_1 (ps)	Δ_2 (cm^{-1})	t_2 (ps)	Δ_s (cm^{-1})	ω_0 (cm^{-1})	a_1	T_1 (ps)
1	76	41	0.38	34	1.7	…	2509	0.56	1.8
2	35	55	1.9	…	…	20	2565	0.44	4.5
2 FFCF	36	60	1.9	…	…	19.3	…	…	…

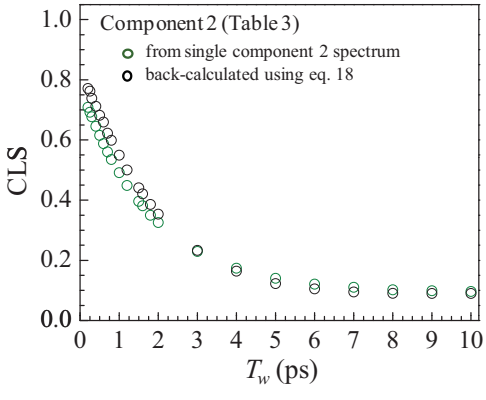

FIG. 12. CLS results for the second model case of overlapping bands (Table III with component 2 center at 2565 cm^{-1}) at T_w = 0.2 ps. The green dots are the CLS from the calculated 2D spectra of component 2 by itself. The black dots are the component 2 results after applying Eq. (18).

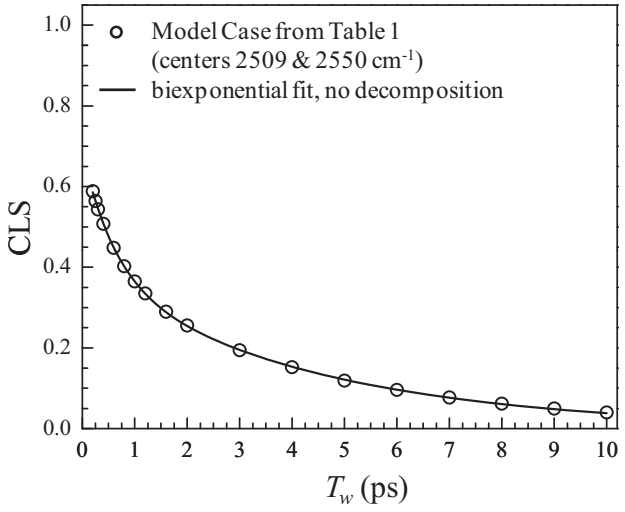

FIG. 13. CLS decay, calculated around the 2D IR maxima, for the first model case (Table I with component 2 center at 2550 cm^{-1}) without decomposing the data into different components. A biexponential fit to the curve yields ambiguous information.

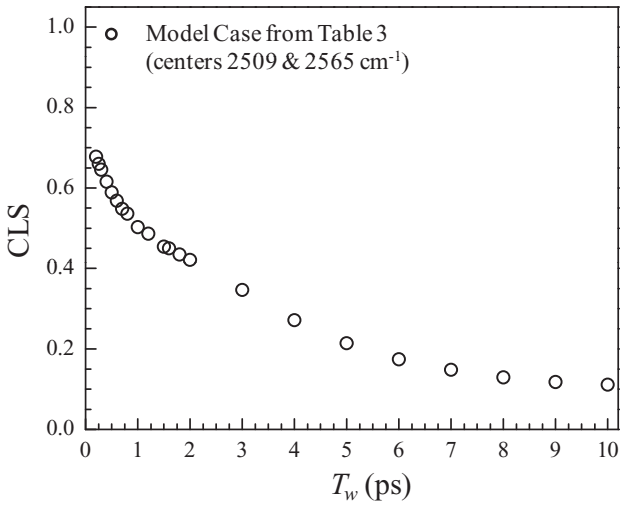

FIG. 14. CLS decay, calculated around the 2D IR maxima, for the second model case (Table III with component 2 center at 2565 cm^{-1}) without decomposing the data into different components. It is unclear what functional form this CLS curve should take, indicating that decomposing the CLS data into separate components can yield more useful information.

cay constants for a given component, respectively. The time constants fall between the known starting values for each component in Table I, but without knowledge of any of the components, no further information can be gained. The fit parameters could be used to calculate an FFCF, but the resulting processes would be nonspecific to the different environments in a system and instead indicate a type of average behavior. Much more information can be gained by separating out the components using Eq. (18).

Figure 14 shows the CLS curve, calculated around the peak position for each spectrum, for the second model case listed in Table III. The resulting curve can be fit to a biexponential plus and offset, but it is unclear what the fit parameters can tell us about the system, since there appears to be a kink in the curve around 2 ps, indicating that a strictly biexponential fit plus offset is not the correct functional form for the FFCF. This is not surprising because the CLS points reflect the combination of two distinct FFCFs. This kink is most likely due to the relatively faster FFCF of bulk water dying out more quickly than the FFCF for component 2. Similar shapes have been observed for multi-component anisotropy decays where one component reorients faster than the second.[39,43,77] Figures 13 and 14 show an important aspect of multi-component systems. In Figure 14, the shape of the CLS data obtained from a series of 2D IR spectra hints the data are not arising from a single component system. However, the plot in Figure 13 does not provide an indication that the system has two components. The curve can be fit very nicely to a sum of exponentials. However, treating the CLS as if it is a one component system does not provide the correct FFCF parameters for either component. Therefore, the algorithm presented in this paper is not a cure-all for ambiguous data sets but rather a tool for analysis of two components systems that can be used when critical pieces of information are known beforehand or can be reasonably simulated.

IV. DEGREE OF ERROR IN THE TWO-COMPONENT CLS METHOD

The model cases discussed above show that in non-overlapping and even in significantly overlapping cases with resolvable 2D IR spectra, the CLS for each component can be directly calculated from the spectra separately for each component. It appears that when the separation of the 0-1 peaks for the two components exceeds 50% of the FWHM of one of the components, then the CLS curves may be calculated directly from the spectra. This is certainly the case for the red and blue states of HRP referenced earlier because the spectral separation is several times larger than the bandwidth of the peaks.[35] Figure 9 suggests that the results are same whether or not the CLS is obtained from the spectra or Eq. (18). In cases where the separation of components is less than 50% of one of the FWHM values, then Eq. (18) should be used to obtain the correct center line data. A general rule of thumb is that if one cannot distinguish separate peaks, then the algorithm should be used.

Another point of interest is how much error can be introduced into the FFCF parameters after doing the simultaneous fit of CLS data and the IR spectrum. The extracted FFCF parameters using Eq. (18) that are presented in Tables II and III show that the parameters are reasonably reproduced when compared to the initial known values for component 2. It should be noted that the algorithm was tested for quite a few other cases not presented here. For example, we tested the algorithm for two components with similar vibrational lifetimes and found no change in accuracy. Throughout our studies, it appeared that the algorithm typically returned Δ values within ± 5 cm^{-1} of the starting value with occasional deviants of ± 10 cm^{-1}. The time constants were generally within ± 1 ps. As can be seen from Tables I and II, there can be great error associated with the homogeneous component, but this degree of error is similar to previously re-

ported error values for the homogeneous component.[11] Overall, the algorithm presented in this paper succeeds in capturing the overall dynamics of a system (biexponential, single exponential, etc.) and returns values that are reasonably close to the true parameters. When applied to experimental systems, results can be trusted and the errors may not exceed experimental error.

V. CONCLUDING REMARKS

2D IR vibrational echo spectroscopy is a useful technique for studying the dynamics of molecules in liquids, solids, and biological systems. The dynamics of a system are described by the frequency-frequency correlation function that can be extracted from the 2D spectra using the CLS technique. The main benefit of the CLS technique is that a full response function calculation is not needed to obtain the full FFCF. In contrast to other methods, the CLS technique is insensitive to pulse duration, Fourier filtering techniques, sloping absorptive background, and the overlap of the 0-1 and 1-2 transition peaks.[10] However, when more than one species is present in a system, the CLS technique becomes more complicated, and normal application of the CLS technique can yield ambiguous information. We have shown mathematically that the peak location of a slice through a spectrum with two components is a weighted combination of the peak locations of the individual components. The center line data (set of peak locations vs. ω_τ for a given T_w) for each component are weighted by frequency and T_w-dependent fraction terms, which can be obtained from the linear absorption spectra and vibrational lifetimes of the two components. Therefore, if one of the components of a two component system is well characterized, and if other parameters for both components are known, i.e., the center frequencies, vibrational lifetimes, and IR spectra, then the set of center line data for the second component can be readily back-calculated (using Eq. (18)) from experimental data of the combined system. After the center line data for component 2 is calculated, CLS analysis may be performed and the FFCF for the second component obtained.

We have tested this algorithm for a variety of model cases to show its accuracy in reproducing sets of model data. Overall, the extracted FFCF parameters of the unknown component are quite accurate. A significant implication of this algorithm is the realization that the CLS curve for a multiple component system is not itself a weighted average of individual CLS curves for each component separately (shown in detail in Appendix). Therefore, a traditional single CLS curve is not very useful in describing the dynamics of a multiple component system. The algorithm developed here extracts an unknown FFCF from a set of 2D IR data consisting of two contributing components.

ACKNOWLEDGMENTS

E. E. F. thanks Daniel Rosenfeld, Amr Tamimi, Daryl Wong, Chiara Giammanco, Jean Chung, and Megan Thielges for useful discussions. We would like to thank the (U.S.) Department of Energy (DOE) (DE-FG03-84ER13251) for support of this research.

APPENDIX: DERIVATION OF THE TWO COMPONENT CLS METHOD

For a two component system, the 2D IR line shape is

$$\begin{aligned} R(\omega_m, \omega_\tau) &= f_1(\omega_\tau, T_w)\left[\frac{4\pi\sqrt{2}}{K_1(T_w)^{1/2}}\exp\left(\frac{A_1(\omega_m,\omega_\tau)}{K_1(T_w)}\right)\right. \\ &\quad \left. -\frac{2\pi s^2\sqrt{2}}{Q_1(T_w)^{1/2}}\exp\left(\frac{B_1(\omega_m,\omega_\tau)}{Q_1(T_w)}\right)\right] \\ &\quad +(1-f_1(\omega_\tau, T_w))\left[\frac{4\pi\sqrt{2}}{K_2(T_w)^{1/2}}\exp\left(\frac{A_2(\omega_m,\omega_\tau)}{K_2(T_w)}\right)\right. \\ &\quad \left. -\frac{2\pi s^2\sqrt{2}}{Q_2(T_w)^{1/2}}\exp\left(\frac{B_2(\omega_m,\omega_\tau)}{Q_2(T_w)}\right)\right], \end{aligned} \tag{A1}$$

where the A_i, B_i, K_i, and Q_i parameters are defined by

$$\begin{aligned} A_i(\omega_m,\omega_\tau) &= -\left(C_1^i(0)\omega_m^2 - 2C_1^i(T_w)\omega_m\omega_\tau + C_1^i(0)\omega_\tau^2\right), \\ B_i(\omega_m,\omega_\tau) &= -\left(C_1^i(0)(\omega_m+\Delta)^2 - 2C_2^i(T_w)(\omega_m+\Delta)\omega_\tau \right. \\ &\quad \left. +C_3^i(0)\omega_\tau^2\right), \\ K_i(T_w) &= \sqrt{C_1^i(0)^2 - C_1^i(T_w)^2}, \\ Q_i(T_w) &= \sqrt{C_1^i(0)C_3^i(0) - C_2^i(T_w)^2}, \end{aligned} \tag{A2}$$

where

$$\begin{aligned} C_1^i(t) &= \left\langle \delta\omega_{10}^i(\tau_1)\delta\omega_{10}^i(0)\right\rangle, \\ C_2^i(t) &= \left\langle \delta\omega_{21}^i(\tau_1)\delta\omega_{10}^i(0)\right\rangle, \\ C_3^i(t) &= \left\langle \delta\omega_{21}^i(\tau_1)\delta\omega_{21}^i(0)\right\rangle. \end{aligned} \tag{A3}$$

The f_1 term corresponds to a frequency and T_w-dependent fraction term. The fraction reflects the overall concentration of a species at a certain wavelength and is given by

$$f_1(\omega_\tau, T_w) = \frac{S_1(\omega_\tau)e^{-T_w/T_1^1}}{S_1(\omega_\tau)e^{-T_w/T_1^1} + S_2(\omega_\tau)e^{-T_w/T_1^2}}, \tag{A4}$$

where S_1 and S_2 are the component linear absorption spectra whose sum yields the linear absorption spectrum of the combined system. T_1^1 and T_1^2 are the vibrational lifetimes of components 1 and 2, respectively.

The location of the maximum of a slice along the ω_m axis is found by setting the partial derivative of Eq. (A1) with respect to ω_m to 0,

$$\frac{\partial R(\omega_m,\omega_\tau)}{\partial \omega_m} = f_1(\omega_\tau,T_w)_1\left[\frac{4\pi\sqrt{2}}{K_1(T_w)^{3/2}}\exp\left(\frac{A_1(\omega_m,\omega_\tau)}{K_1(T_w)}\right)\frac{\partial A_1(\omega_m,\omega_\tau)}{\partial\omega_m} - \frac{2\pi s^2\sqrt{2}}{Q_1(T_w)^{3/2}}\exp\left(\frac{B_1(\omega_m,\omega_\tau)}{Q_1(T_w)}\right)\frac{\partial B_1(\omega_m,\omega_\tau)}{\partial\omega_m}\right] + (1-f_1(\omega_\tau,T_w))\left[\frac{4\pi\sqrt{2}}{K_2(T_w)^{3/2}}\exp\left(\frac{A_2(\omega_m,\omega_\tau)}{K_2(T_w)}\right)\frac{\partial A_2(\omega_m,\omega_\tau)}{\partial\omega_m} - \frac{2\pi s^2\sqrt{2}}{Q_2(T_w)^{3/2}}\exp\left(\frac{B_2(\omega_m,\omega_\tau)}{Q_2(T_w)}\right)\frac{\partial B_2(\omega_m,\omega_\tau)}{\partial\omega_m}\right] = 0 \tag{A5}$$

where the A_i, B_i, K_i, and Q_i parameters are defined by Eqs. (A2) and (A3).

Equation (A5) defines a set of ω_m and ω_τ values that correspond to the location of the maximum along a slice parallel to ω_m. We can take the derivative of Eq. (A5) with respect to ω_τ to obtain an equation for the slope of the curve created by the maxima locations. After extensive rearrangement of Eq. (A5) and using the harmonic approximation for each set of correlation functions associated with a given component, we obtain the following expression for $\frac{d\omega_m}{d\omega_\tau}$:

$$\frac{d\omega_m}{d\omega_\tau} = \frac{f_1(\omega_\tau,T_w)F(\omega_m,\omega_\tau,T_w,s) - G(\omega_m,\omega_\tau,T_w,s)\frac{df_1}{d\omega_\tau}}{f_1(\omega_\tau,T_w)J(\omega_m,\omega_\tau,T_w,s)+(1-f_1(\omega_\tau,T_w))K(\omega_m,\omega_\tau,T_w,s)} + \frac{(1-f_1(\omega_\tau,T_w))H(\omega_m,\omega_\tau,T_w,s)+I(\omega_m,\omega_\tau,T_w,s)\frac{df_1}{d\omega_\tau}}{f_1(\omega_\tau,T_w)J(\omega_m,\omega_\tau,T_w,s)+(1-f_1(\omega_\tau,T_w))K(\omega_m,\omega_\tau,T_w,s)}. \tag{A6}$$

Equation (A6) is written in a highly condensed form where

$$F(\omega_m,\omega_\tau,T_w,s) = \frac{-2C_1^1(T_w)e^{a/b}}{\left(C_1^1(0)^2-C_1^1(T_w)^2\right)^{3/2}} + \frac{4e^{a/b}\left(-C_1^1(0)\omega_m+C_1^1(T_w)\omega_\tau\right)\left(-C_1^1(T_w)\omega_m+C_1^1(0)\omega_\tau\right)}{\left(C_1^1(0)^2-C_1^1(T_w)^2\right)^{5/2}} + \frac{2s^2e^{c/b}\left(C_1^1(T_w)\omega_m-C_1^1(0)(\omega_m+\Delta)\right)\left(-C_1^1(0)\omega_\tau+C_1^1(T_w)(\omega_m+\Delta)\right)}{\left(C_1^1(0)^2-C_1^1(T_w)^2\right)^{5/2}}, \tag{A7}$$

$$G(\omega_m,\omega_\tau,T_w,s) = \frac{2e^{a/b}\left(-C_1^1(0)\omega_m+C_1^1(T_w)\omega_\tau\right)}{\left(C_1^1(0)^2-C_1^1(T_w)^2\right)^{3/2}} - \frac{e^{c/b}s^2\left(C_1^1(T_w)\omega_m-C_1^1(0)(\omega_m+\Delta)\right)}{\left(C_1^1(0)^2-C_1^1(T_w)^2\right)^{3/2}}, \tag{A8}$$

$$H(\omega_m,\omega_\tau,T_w,s) = \frac{2C_1^2(T_w)e^{d/f}}{\left(C_1^2(0)^2-C_1^2(T_w)^2\right)^{3/2}} + \frac{4e^{d/f}\left(-C_1^2(0)\omega_m+C_1^2(T_w)\omega_\tau\right)\left(-C_1^2(T_w)\omega_m+C_1^2(0)\omega_\tau\right)}{\left(C_1^2(0)^2-C_1^2(T_w)^2\right)^{5/2}} + \frac{2s^2e^{g/f}\left(C_1^2(T_w)\omega_m-C_1^2(0)(\omega_m+\Delta)\right)\left(-C_1^2(0)\omega_\tau+C_1^2(T_w)(\omega_m+\Delta)\right)}{\left(C_1^2(0)^2-C_1^2(T_w)^2\right)^{5/2}}, \tag{A9}$$

$$I(\omega_m,\omega_\tau,T_w,s) = \frac{2e^{d/f}\left(-C_1^2(0)\omega_m+C_1^2(T_w)\omega_\tau\right)}{\left(C_1^2(0)^2-C_1^2(T_w)^2\right)^{3/2}} - \frac{e^{g/f}s^2\left(C_1^2(T_w)\omega_m-C_1^2(0)(\omega_m+\Delta)\right)}{\left(C_1^2(0)^2-C_1^2(T_w)^2\right)^{3/2}}, \tag{A10}$$

$$J(\omega_m,\omega_\tau,T_w,s) = \frac{-2C_1^1(0)c^{a/b}}{\left(C_1^1(0)^2-C_1^1(T_w)^2\right)^{3/2}} + \frac{e^{c/b}s^2\left(C_1^1(0)-C_1^1(T_w)\right)}{\left(C_1^1(0)^2-C_1^1(T_w)^2\right)^{3/2}} + \frac{4e^{a/b}\left(-C_1^1(0)\omega_m+C_1^1(T_w)\omega_\tau\right)^2}{\left(C_1^1(0)^2-C_1^1(T_w)^2\right)^{5/2}} + \frac{2e^{c/b}s^2\left(C_1^1(T_w)\omega_m-C_1^1(0)(\omega_m+\Delta)\right)\left(C_1^1(0)(\omega_m+\Delta)-C_1^1(T_w)\omega_\tau\right)}{\left(C_1^1(0)^2-C_1^1(T_w)^2\right)^{5/2}}, \tag{A11}$$

$$K(\omega_m, \omega_\tau, T_w, s) = \frac{-2C_1^2(0)c^{d/f}}{\left(C_1^2(0)^2 - C_1^2(T_w)^2\right)^{3/2}} + \frac{e^{g/f}s^2\left(C_1^2(0) - C_1^2(T_w)\right)}{\left(C_1^2(0)^2 - C_1^2(T_w)^2\right)^{3/2}}$$
$$+\frac{4e^{d/f}\left(-C_1^2(0)\omega_m + C_1^2(T_w)\omega_\tau\right)^2}{\left(C_1^2(0)^2 - C_1^2(T_w)^2\right)^{5/2}}$$
$$+\frac{2e^{g/f}s^2\left(C_1^2(T_w)\omega_m - C_1^2(0)(\omega_m + \Delta)\right)\left(C_1^2(0)(\omega_m + \Delta) - C_1^2(T_w)\omega_\tau\right)}{\left(C_1^2(0)^2 - C_1^2(T_w)^2\right)^{5/2}}, \tag{A12}$$

and

$$a = -C_1^1(0)\omega_m^2 + 2C_1^1(T_w)\omega_m\omega_\tau - C_1^1(0)\omega_\tau^2, \tag{A13}$$

$$b = C_1^1(0)^2 - C_1^1(T_w)^2, \tag{A14}$$

$$c = -C_1^1(0)^2 + 2C_1^1(T_w)\omega_\tau(\omega_m + \Delta) - C_1^1(0)(\omega_m + \Delta)^2, \tag{A15}$$

$$d = -C_1^2(0)\omega_m^2 + 2C_1^2(T_w)\omega_m\omega_\tau - C_1^2(0)\omega_\tau^2, \tag{A16}$$

$$f = C_1^2(0)^2 - C_1^2(T_w)^2, \tag{A17}$$

$$g = -C_1^2(0)^2 + 2C_1^2(T_w)\omega_\tau(\omega_m + \Delta) - C_1^2(0)(\omega_m + \Delta)^2. \tag{A18}$$

In these expressions, the C_1^i terms are correlation functions for the ith component.

Equation (A6) is not a very practical expression, especially for use in analyzing 2D spectra. It is extremely important to note that the resulting slope is not simply a weighted average of the slopes of both components. The center line data points are, however, a weighted average of the center line data points for each component. If a center line point corresponding to a maximum along ω_m is denoted as ω_m^*, then this relationship may be mathematically expressed by

$$\omega_{mC}^*(\omega_m, \omega_\tau, T_w) = f_1(\omega_\tau, T_w)\omega_{m1}^*(\omega_m, \omega_\tau, T_w) + (1 - f_1(\omega_\tau, T_w))\omega_{m2}^*(\omega_m, \omega_\tau, T_w), \tag{A19}$$

where ω_{mC}^*, ω_{m1}^*, and ω_{m2}^* represent the sets of center line data for the experimentally observed two component system, component 1 by itself, and component 2 by itself, respectively. Differentiating Eq. (A20) with respect to ω_τ recovers Eq. (A7),

$$\frac{d\omega_{mC}^*}{d\omega_\tau} = f_1(\omega_\tau, T_w)\frac{d\omega_{m1}^*}{d\omega_\tau} + \omega_{m1}^*(\omega_m, \omega_\tau, T_w)\frac{df_1}{d\omega_\tau} + (1 - f_1(\omega_\tau, T_w))\frac{d\omega_{m2}^*}{d\omega_\tau} - \omega_{m2}^*(\omega_m, \omega_\tau, T_w)\frac{df_1}{d\omega_\tau}. \tag{A20}$$

If one of the components is completely known, that is, the center line data can be measured or simulated independently from the combined system, then the second component may be calculated from,

$$\omega_{m2}^*(\omega_m, \omega_\tau, T_w) = \frac{\left(\omega_{m2C}^*(\omega_m, \omega_\tau, T_w) - f_1(\omega_\tau, T_w)\omega_{m1}^*(\omega_m, \omega_\tau, T_w)\right)}{(1 - f_1(\omega_\tau, T_w))}. \tag{A21}$$

The details surrounding the use of Eq. (A21) have been discussed in the main text.

[1] J. Zheng, K. Kwak, and M. D. Fayer, Acc. Chem. Res. **40**, 75 (2007).
[2] R. M. Hochstrasser, Adv. Chem. Phys. **132**, 1 (2006).
[3] S. Mukamel, *Principles of Nonlinear Optical Spectroscopy* (Oxford University Press, New York, 1995).
[4] S. Mukamel, Ann. Rev. Phys. Chem. **51**, 691 (2000).
[5] M. Khalil, N. Demirdoven, and A. Tokmakoff, J. Phys. Chem. A **107**, 5258 (2003).
[6] C. J. Fecko, J. J. Loparo, S. T. Roberts, and A. Tokmakoff, J. Chem. Phys. **122**, 054506 (2005).
[7] J. B. Asbury, T. Steinel, K. Kwak, S. A. Corcelli, C. P. Lawrence, J. L. Skinner, and M. D. Fayer, J. Chem. Phys. **121**, 12431 (2004).
[8] J. B. Asbury, T. Steinel, C. Stromberg, S. A. Corcelli, C. P. Lawrence, J. L. Skinner, and M. D. Fayer, J. Phys.Chem. A **108**, 1107 (2004).
[9] K. Kwak, S. Park, I. J. Finkelstein, and M. D. Fayer, J. Chem. Phys. **127**, 124503 (2007).
[10] K. Kwak, D. E. Rosenfeld, and M. D. Fayer, J. Chem. Phys. **128**(20), 204505 (2008).
[11] S. Park and M. D. Fayer, Proc. Natl. Acad. Sci. U.S.A. **104**(43), 16731 (2007).
[12] R. A. Nicodemus, K. Ramasesha, S. T. Roberts, and A. Tokmakoff, J. Phys. Chem. Lett. **1**(7), 1068 (2010).
[13] M. L. Cowan, B. D. Bruner, N. Huse, J. R. Dwyer, B. Chugh, E. T. J. Nibbering, T. Elsaesser, and R. J. D. Miller, Nature (London) **434**(7030), 199 (2005).
[14] J. J. Loparo, S. T. Roberts, and A. Tokmakoff, J. Chem. Phys. **125**, 194521 (2006).
[15] J. J. Loparo, S. T. Roberts, and A. Tokmakoff, J. Chem. Phys. **125**, 194522 (2006).
[16] J. B. Asbury, T. Steinel, C. Stromberg, K. J. Gaffney, I. R. Piletic, and M. D. Fayer, J. Chem. Phys. **119**(24), 12981 (2003).
[17] S. T. Roberts, K. Ramasesha, P. B. Petersen, A. Mandal, and A. Tokmakoff, J. Phys. Chem. A **115**(6), 3957 (2011).
[18] Z. Ganim, K. C. Jones, and A. Tokmakoff, Phys. Chem. Chem. Phys. **12**, 3579 (2010).
[19] I. J. Finkelstein, J. Zheng, H. Ishikawa, S. Kim, K. Kwak, and M. D. Fayer, Phys. Chem. Chem. Phys. **9**, 1533 (2007).
[20] L. P. DeFlores, Z. Ganim, S. F. Ackley, H. S. Chung, and A. Tokmakoff, J. Phys. Chem. B **110**, 18973 (2006).

[21]P. Mukherjee, I. Kass, I. T. Arkin, and M. T. Zanni, Proc. Natl. Acad. Sci. U.S.A. **103**(10), 3528 (2006).
[22]H. Ishikawa, K. Kwak, J. K. Chung, S. Kim, and M. D. Fayer, Proc. Natl. Acad. Sci. U.S.A. **105**(25), 8619 (2008).
[23]M. C. Thielges, J. K. Chung, and M. D. Fayer, J. Am. Chem. Soc. **133**(11), 3995 (2011).
[24]J. K. Chung, M. C. Thielges, S. J. Bowman, K. L. Bren, and M. D. Fayer, J. Am. Chem. Soc. **133**(17), 6681 (2011).
[25]J. K. Chung, M. C. Thielges, and M. D. Fayer, Proc. Natl. Acad. Sci. U.S.A. **108**(9), 3578 (2011).
[26]M. J. Tucker, X. S. Gai, E. E. Fenlon, S. H. Brewer, and R. M. Hochstrasser, Phys. Chem. Chem. Phys. **13**, 2237 (2011).
[27]D. E. Moilanen, D. Wong, D. E. Rosenfeld, E. E. Fenn, and M. D. Fayer, Proc. Natl. Acad. Sci. U.S.A. **106**(2), 375 (2009).
[28]Y. S. Kim and R. M. Hochstrasser, Proc. Natl. Acad. Sci. U.S.A. **102**, 11185 (2005).
[29]J. Zheng, K. Kwak, J. B. Asbury, X. Chen, I. R. Piletic, and M. D. Fayer, Science **309**(5739), 1338 (2005).
[30]K. Kwak, J. Zheng, H. Cang, and M. D. Fayer, J. Phys. Chem. B **110**, 19998 (2006).
[31]J. Zheng, K. Kwak, J. Xie, and M. D. Fayer, Science **313**, 1951 (2006).
[32]D. E. Rosenfeld, K. Kwak, Z. Gengeliczki, and M. D. Fayer, J. Phys. Chem. B **114**, 2383 (2010).
[33]S. Mukamel and R. F. Loring, J. Opt. Soc. B **3**, 595 (1986).
[34]S. T. Roberts, J. J. Loparo, and A. Tokmakoff, J. Chem. Phys. **125**(8), 084502 (2006).
[35]I. J. Finkelstein, H. Ishikawa, S. Kim, A. M. Massari, and M. D. Fayer, Proc. Nat. Acad. Sci. U.S.A. **104**, 2637 (2007).
[36]C. Fang, J. D. Bauman, K. Das, A. Remorino, A. Arnold, and R. M. Hochstrasser, Proc. Nat. Acad. Sci. U.S.A. **105**, 1472 (2008).
[37]D. Kraemer, M. L. Cowan, A. Paarman, N. Huse, E. T. J. Nibbering, T. Elsaesser, and R. J. D. Miller, Proc. Natl. Acad. Sci. U.S.A. **105**(2), 437 (2008).
[38]E. E. Fenn, D. B. Wong, and M. D. Fayer, J. Chem. Phys. **134**, 054512 (2011).
[39]D. E. Moilanen, E. E. Fenn, D. Wong, and M. D. Fayer, J. Phys. Chem. B **113**, 8560 (2009).
[40]D. E. Moilanen, E. E. Fenn, D. Wong, and M. D. Fayer, J. Am. Chem. Soc. **131**, 8318 (2009).
[41]D. E. Moilanen, E. E. Fenn, D. Wong, and M. D. Fayer, J. Chem. Phys. **131**, 014704 (2009).
[42]D. E. Moilanen, N. Levinger, D. B. Spry, and M. D. Fayer, J. Am. Chem. Soc. **129** (46), 14311 (2007).
[43]E. E. Fenn, D. B. Wong, and M. D. Fayer, Proc. Nat. Acad. Sci. U.S.A. **106**, 15243 (2009).
[44]D. Cringus, A. Bakulin, J. Lindner, P. Vohringer, M. S. Pshenichnikov, and D. A. Wiersma, J. Phys. Chem. B **111**(51), 14193 (2007).
[45]D. Cringus, J. Lindner, M. T. W. Milder, M. S. Pshenichnikov, P. Vohringer, and D. A. Wiersma, Chem. Phys. Lett. **408**, 162 (2005).
[46]A. M. Dokter, S. Woutersen, and H. J. Bakker, Phys. Rev. Lett. **94**, 178301 (2005).
[47]A. M. Dokter, S. Woutersen, and H. J. Bakker, Proc. Nat. Acad. Sci. U.S.A. **103**, 15355 (2006).
[48]A. M. Dokter, S. Woutersen, and H. J. Bakker, J. Chem. Phys. **126**(12) (2007).
[49]I. R. Piletic, D. E. Moilanen, D. B. Spry, N. E. Levinger, and M. D. Fayer, J. Phys. Chem. A **110**, 4985 (2006).
[50]I. R. Piletic, H.-S. Tan, and M. D. Fayer, J. Phys. Chem. B **109**(45), 21273 (2005).
[51]H.-S. Tan, I. R. Piletic, and M. D. Fayer, J. Chem. Phys. **122**, 174501(9) (2005).
[52]H.-S. Tan, I. R. Piletic, R. E. Riter, N. E. Levinger, and M. D. Fayer, Phys. Rev. Lett. **94**, 057405 (2005).
[53]P. Grigolini and M. Maestro, Chem. Phys. Lett. **123**(3), 248 (1986).
[54]P.-O. Quist and B. Halle, J. Chem. Soc. Faraday Trans. 1 **84**(4), 1033 (1988).
[55]D. Pant, R. E. Riter, and N. E. Levinger, J. Chem. Phys. **109**, 9995 (1998).
[56]R. E. Riter, E. P. Undiks, and N. E. Levinger, J. Am. Chem. Soc. **120**, 6062 (1998).
[57]N. E. Levinger, Curr. Opin. Colloid Interface Sci. **5**, 118 (2000).
[58]N. E. Levinger, Science **298**, 1722 (2002).
[59]A. Douhal, G. Angulo, M. Gil, J. A. Organero, M. Sanz, and L. Tormo, J. Phys. Chem. B **111**(19), 5487 (2007).
[60]M. Ueda and Z. A. Schelly, Langmuir **5**(4), 1005 (1989).
[61]P. E. Zinsli, J. Phys. Chem. **83**(25), 3223 (1979).
[62]K. Bhattacharyya, Acc. Chem. Res. **36**(2), 95 (2003).
[63]M. R. Harpham, B. M. Ladanyi, N. E. Levinger, and K. W. Herwig, J. Chem. Phys. **121**, 7855 (2004).
[64]N. Nandi, K. Bhattacharyya, and B. Bagchi, Chem. Rev. **100**(6), 2013 (2000).
[65]B. Baruah, J. M. Roden, M. Sedgwick, N. M. Correa, D. C. Crans, and N. E. Levinger, J. Am. Chem. Soc. **128**(39), 12758 (2006).
[66]D. C. Crans, C. D. Rithner, B. Baruah, B. L. Gourley, and N. E. Levinger, J. Am. Chem. Soc. **128**(13), 4437 (2006).
[67]M. Zulauf and H. F. Eicke, J. Phys. Chem. **83**(4), 480 (1979).
[68]T. Kinugasa, A. Kondo, S. Nishimura, Y. Miyauchi, Y. Nishii, K. Watanabe, and H. Takeuchi, Colloids Surf., A **204**(1–3), 193 (2002).
[69]H.-F. Eicke and J. Rehak, Helv. Chim. Acta **59**(8), 2883 (1976).
[70]J. R. Schmidt, S. A. Corcelli, and J. L. Skinner, J. Chem. Phys. **123**, 044513(13) (2005).
[71]J. R. Schmidt, S. T. Roberts, J. J. Loparo, A. Tokmakoff, M. D. Fayer, and J. L. Skinner, Chem. Phys. **341**, 143 (2007).
[72]M. H. Cho, J. Y. Yu, T. H. Joo, Y. Nagasawa, S. A. Passino, and G. R. Fleming, J. Phys. Chem. **100**(29), 11944 (1996).
[73]K. J. Gaffney, I. R. Piletic, and M. D. Fayer, J. Chem. Phys. **118**, 2270 (2003).
[74]S. Woutersen and H. J. Bakker, Nature (London) **402**(6761), 507 (1999).
[75]J. Sung and R. J. Silbey, J. Chem. Phys. **115**, 9266 (2001).
[76]O. Golonzka, M. Khalil, N. Demirdoven, and A. Tokmakoff, J. Chem. Phys. **115**, 10814 (2001).
[77]E. E. Fenn, D. E. Moilanen, N. E. Levinger, and M. D. Fayer, J. Am. Chem. Soc. **131**, 5530 (2009).